A soft template approach to various porous nanostructures from conjugated carbazole-based monomers

Caroline Fradin, Frédéric Guittard, Thierry Darmanin

Graphical Abstract

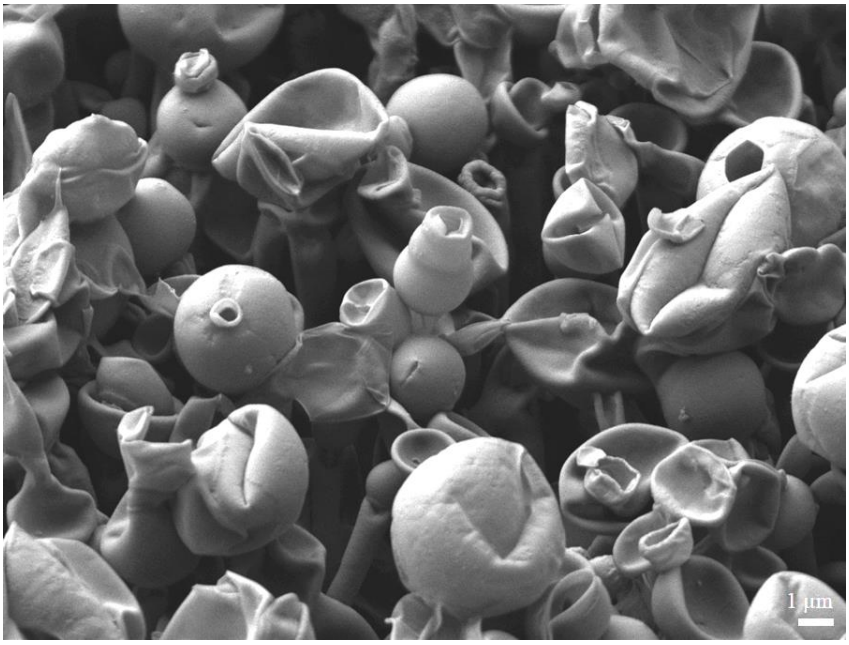

A soft template approach to various porous nanostructures from conjugated carbazole-based monomers

Caroline Fradin, Frédéric Guittard and Thierry Darmanin*

Université Côte d'Azur, NICE Lab, 28 avenue Valrose, 06100 Nice, France.

Corresponding author: thierry.darmanin@unice.fr ; Tel : +33 6 34 12 10 13.

Abstract

Hypothesis

Controlling the size and the shape of nanostructures on surfaces is fundamental for various applications while the formation of porous structures such as nanotubes is particularly difficult. The templateless electropolymerization is a choice process that not only forms nanostructured surfaces, but also can tune their morphologies using different monomers.

Experiments

In this work, we used this soft-template and surfactant free electropolymerization in organic solvent to deposit for the first time carbazole-based monomers. Five different conjugated carbazole-based monomers are tested here.

Findings

We show that the shape of surfaces nanostructures is highly dependent on the amount of water present in the organic solvent and on the molecular structure of the carbazole monomers. Different morphologies are obtained from fibers to vertically aligned nanotubes and even porous membranes, depending on the monomer and on the electropolymerization method. The nanostructured surfaces reach superhydrophobic properties and their dynamical non-wetting behavior varies with the monomer and the electrochemical parameters.

Keywords: Superhydrophobic, Wettability, Electropolymerization, Conducting polymers, Carbazole.

1. Introduction

Nanostructured and porous surfaces are used in various applications such as optical and electronic devices, biomedical sensors, as well as surface wetting properties [1–5]. Natural hydrophobic surfaces exhibit indeed such micro/nanostructures which turned out to be essential in their non wetting capability. [6–8]. The impact of the surface roughness can be explained by the Wenzel and Cassie-Baxter models [9–14]. The lotus leaves are the most known example of biomimicry for wetting properties.

Such structured surfaces are however difficult to realize and especially when the nanostructures have geometrical shapes as nanotubes. Although many methods exist such as electrospinning, lithography or anodization [15,16], they are difficult to implement and often need the use of hard templates. The templateless electropolymerization method is a fast way to produce very ordered porous nanostructured polymer films with various geometrical shapes and doesn't require any hard template. In this soft templating approach, gas bubbles released *in-situ* during electropolymerization are indeed held responsible for the formation of porous structures like nanotubes [17–22]. In water (H_2O), porous structures were reported especially with pyrrole as monomer but a surfactant is needed to stabilize the gas bubbles (O_2 and/or H_2

depending on the electropolymerization method) released by the water oxidation and/or reduction. This method has also been reported in organic solvent like dichloromethane (CH_2Cl_2) and without surfactant with different conductive polymers such as poly(3,4-phenylenedioxythiophene), poly(3,4-naphthalenedioxythiophene), and recently thienothiophenes [23–29], giving surfaces with strong water adhesion.

The morphologies of the polymer depositions can by this way be adjusted by the nature of the monomer. However, in order to control the surface behavior of liquids of lower surface tension than water, such as oils, it would be preferable to use in the future other monomers of higher polarity compared to thiophene-based monomers. The highest superoleophobic properties were indeed obtained with fluorinated 3,4-ethylenedioxypyrrole (EDOP) derivatives [30]. Because we demonstrated that the presence of aromatic groups favoring π-sticking interactions often gives the best results, we chose here to study carbazole-based monomers (two benzene rings fused on pyrrole). Moreover, we also showed that carbazole can give exceptional results when it is used as a substituent on monomers, comparable to pyrene [31].

Nevertheless, carbazole is *a priori* not a good candidate to form conducting polymer films by electropolymerization because it has many polymerization sites and often leads to short oligomers of high solubility [32]. However, when carbazole is substituted by aromatic groups favoring π-stacking interactions, conducting polymer films can be obtained if these interactions sufficiently decrease the polymer solubility. For example, conjugated carbazoles such as 1,3-bis(*N*-carbazolyl)benzene (mCP), 3,3'-di(9*H*-carbazol-9-yl)-1,1'-biphenyl (mCBP) and 4,4'-bis(*N*-carbazolyl)-1,1'-biphenyl (pCBP) could be good candidates. They are highly conductive monomers which electrochemical properties have been extensively studied for their use in organic light emitting diodes (OLEDs). Their electropolymerized thin films have been only used for their electronic properties as hole transporter and host for phosphorescent dopants [33–36], but not for their capacity to form nanostructured surfaces. Microporous conjugated carbazole-based polymers have also been widely studied for photocatalytic or gas uptake applications [37,38] but such powders are produced by oxidative coupling polymerization [39].

In this manuscript, we study for the first time conjugated carbazoles by this soft templating approach and use these monomers mCP, mCBP, pCBP and CTP (**Figure 1**). Nanostructured surfaces with various static and dynamic hydrophobicity and even super-hydrophobicity are obtained. The similarity between the studied molecules allow to understand the link between their molecular structure and the morphologies of the surfaces.

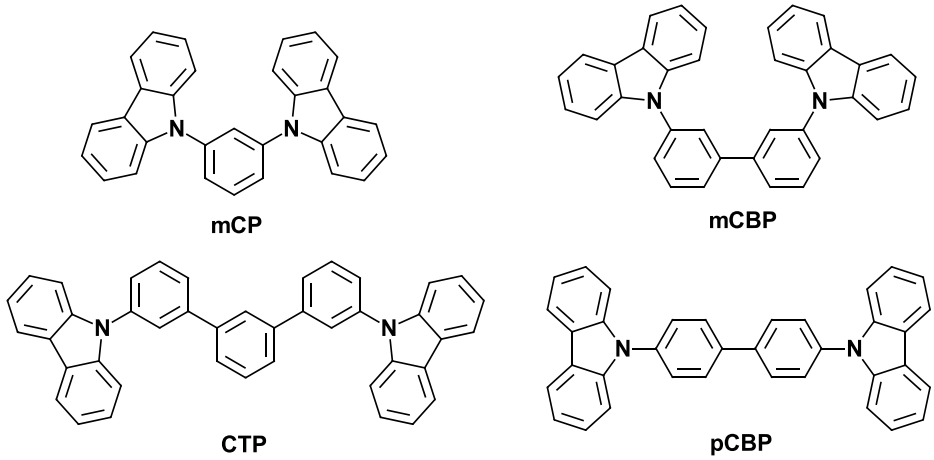

Figure 1. Monomers studied in this manuscript.

2. Materials and Method

2.1. Electropolymerization parameters

The monomers were purchased from Sigma Aldrich Merck and TCI and used as received. The polymers were electrodeposited on gold plates. The electrodepositions were performed with an Autolab potentiostat of Metrohm (Autolab) using a three-electrode system: the gold plate as working electrode, a carbon rod as counter-electrode and a saturated calomel electrode (SCE) as reference electrode. A solution of 0.1 M tetrabutylammonium perchlorate (Bu_4NClO_4) and 0.005 M of monomer was used. The solvent used here was either anhydrous dichloromethane or dichloromethane saturated with water, (called here $CH_2Cl_2 + H_2O$), which was prepared mixing some CH_2Cl_2 and a huge amount of H_2O and collecting the organic phase. Here, H_2O was added to anhydrous CH_2Cl_2 in order to release a much higher amount of O_2 and H_2 bubbles, depending on the polymerization method as reported in the literature [26,40]. Then, the electrodepositions were performed by cyclic voltammetry from -1 V to the first oxidation wave of the monomers (**Table 1**) and at a scan rate of 20 mV s^{-1}. Different number of scans were performed (1, 3 and 5) in order to better investigate the polymer growth. Electrodepositions at constant potential (E_{ox}) were also realized using deposition charges between 12.5 and 400 mC cm^{-2}.

Smooth polymer surfaces were also prepared in order to estimate the effect of surface roughness and determine their surface energy (γ_S) using the Wu equation [41]. Here, smooth polymer surfaces were prepared at constant potential, using an ultra-short deposition charge (2 mC cm^{-2}) and one reduction scans from E^{ox} to -1V in order to reduce the polymer.

Monomers properties			Polymers properties			
nomenclature		E_{ox} (V/SCE)	E_{ox}^1 (V/SCE)	E_{ox}^2 (V/SCE)	E_{red}^1 (V/SCE)	E_{red}^2 (V/SCE)
mCP	1,3-bis(*N*-carbazolyl)benzene	1.87	1.41	1.83	1.00	0.77
mCBP	3,3'-di(9*H*-carbazol-9-yl)-1,1'-biphenyl	1.67	1.21	1.57	1.04	0.82
pCBP	4,4'-bis(*N*-carbazolyl)-1,1'-biphenyl	1.75	1.30	1.79	0.98	0.70
CTP	3,3"-di(9*H*-carbazol-9-yl)-1,1':3',1"-terphenyl	1.60	1.52	1.93	1.16	0.88

Table 1: Peak potentials of electrochemically reversible processes obtained by cyclovoltammetry with the monomers and the polymers films.

2.2. Surface characterization

The contact angle measurements were performed using a DSA30 goniometer of Bruker. The static contact angles were determined with the sessile method using 2 μL droplets of probe liquids of various surface tensions: water (72.8 mN/m), diiodomethane (50.8 mN/m), hexadecane (27.6 mN/m). The dynamic contact angles were determined using the tilted-drop method. In this method, a 6 µL droplet is placed on the surface and the surface is inclined until the droplet moves. Just before the droplet moving, the advanced (θ_{adv}) and receding (θ_{rec}) contact angles are taken and therefore the hysteresis H = θ_{adv} - θ_{rec}. The maximum inclination angle is called sliding angle (α).

The surface energy of the polymer films was calculated using the Wu model with contact angles of water and diiodomethane on the smooth depositions. The Wu model [41] is derived from Owens-Wendt one, where the surface energies are separated into a polar part γ^P and a dispersive part γ^D. The following Wu equation $\gamma_{LV}(1+\cos\theta) = 4\frac{\gamma_{LV}^D\gamma_{SV}^D}{\gamma_{LV}^D+\gamma_{SV}^D} + 4\frac{\gamma_{LV}^P\gamma_{SV}^P}{\gamma_{LV}^P+\gamma_{SV}^P}$. is applied to the two different liquids, and the solid surface energy $\gamma_{SV} = \gamma_{SV}^D + \gamma_{SV}^P$ is calculated resolving a system of the 2 preceding equations. In our case, γ^D_{SV} and γ^P_{SV} were directly obtained using the software "Drop Shape Analysis".

The morphology was evaluated by the scanning electron microscopy (SEM) using a 276 JEOL 6700F microscope on dried polymer films.

The arithmetic (R_a) and quadratic (R_q) surface roughness were obtained with a WYKO NT1100 optical profiling system from Bruker. For these measurements, the working mode HighMag Phase Shift Interference (PSI), the objective 50x, and the field of view 0.5x were used.

IR spectra were performed on a Spectrum 100 FT-IR spectrometer (Perkin Elmer,USA) with a diamond attenuated total reflectance (ATR) top plate accessory. The samples were scanned 3 times at 1 cm^{-1} spectral resolution over the range of 450 cm^{-1} to 4000 cm^{-1}. The spectra reported in this paper were obtained by subtracting the background spectra from the measured spectra.

3. Results and Discussion

3.1. Electrochemical characterization

Monomers were electropolymerized on gold plates by cyclic voltammetry in both solvents CH_2Cl_2 and CH_2Cl_2+H_2O. Most of the monomers presented several oxidation waves between 1 and 3 V vs SCE (**Figure 2 A**) corresponding to the oxidation of the different conducting groups composing the monomer. These molecules are indeed not planar, so that every planar part forms an isolated conjugating system and has it particular oxidation potential [32]. The only monomer presenting a unique oxidation wave between -1 and 3V is mCP. Either this molecule is enough conjugated to present a unique oxidation potential, else the potentials are too close to be distinguished. Because these monomers are meant to polymerize via the carbazole moieties and carbazoles units are known to have a lower oxidation potential than benzene rings [42], we limited the cyclic voltammetry (CV) scans to the lowest oxidation waves.

On CV curves, first scans (in red on **Figure 2**) show one oxidation peak and its complementary reduction peaks attributed to the formation of carbazoles radical cations and their reduction. On this first scan, another reduction wave appears at lower potential. The following scans show the complementary oxidation wave at a lower potential than the first one. These second oxidation and reduction processes are typical of carbazole derivates which undergo a dimerization reaction via the carbazole radical cations [43]. The obtained dimer is more conjugated, so its oxidation occurs at a lower potential and is observed on the following scans.

Water reduction was always quite visible on the CV curves especially in solvent CH_2Cl_2+H_2O. Water in the solvent CH_2Cl_2+H_2O is indeed oxidized in O_2 around 2.5 V/SCE and reduced in H_2 around -0,5 V/SCE [31]. Since the electrodepositions were performed under 2 V vs SCE, the water reduction which emits H_2 gas, is here hold the main responsible for the formation of nanoporous structures on the polymer surfaces [26,40].

The four monomers dimerized the same way *via* the 3rd or 6th carbon of the carbazole units, since the nitrogen atom is already occupied [32]. mCP and pCBP had the highest intensities on CV curves, which means that a higher quantity of polymer was deposited on the electrode. Their depositions were indeed relatively thick and their roughness higher than the two others (**Table 3**).

The electrochemical behavior of the electrodeposited polymer films was also investigated by CV in a monomer free solution of Bu_4NClO_4 as electrolyte in CH_2Cl_2 (**Figure 2 B**). Quantitative details are summarized in **Table 1**. mCP and pCBP films showed two similar reversible oxidation waves, as for polycarbazole [44], at a slightly lower potential for pCBP. However they started to oxidize at a similar potential (E_{onset}(pCBP) = 0.89 V/SCE and E_{onset}(mCP) = 0.90 V/SCE). mCBP and CTP depositions also showed two main reversible oxidation waves but some additional peaks with less intensity were also visible ($E_{ad.\ ox}$(mCBP)=1.03 V/SCE and $E_{ad.\ red}$(mCBP)=1.46 V/SCE and $E_{ad.\ ox}^{1}$(CTP)=1.02 V/SCE, $E_{ad.\ ox}^{2}$(CTP)=1.11 V/SCE and $E_{ad.\ red}^{1}$(CTP)=1.64 V/SCE, $E_{ad.\ red}^{2}$(CTP)=1.38 V/SCE). The processes for additional peaks remain difficult to interpret. The onsets potentials are similar for every polymer (E_{onset}(mCBP) = 0.87 V/SCE and E_{onset}(CTP) = 0.85 V/SCE).

The polymer films were characterized by infrared spectroscopy. The spectra are very similar (**Supporting Information Fig. 1**) since the molecular structures of the monomers are very close. Stretching vibrations of the aromatic carbon double bonds are observed at around 1490, 1590 and 1600-1620 cm^{-1}. Peaks at 1220 and 1327 cm-1 corresponds to the vibrations of the amine bonds of the carbazole moieties. Vibrations of the aromatic C-H bonds of both the carbazole and benzene moieties are observed between 600 and 900 cm^{-1} with main peaks at 625, 700, 745, 760, 800 and 880 cm^{-1}, and between 2870 and 3000 cm^{-1}.

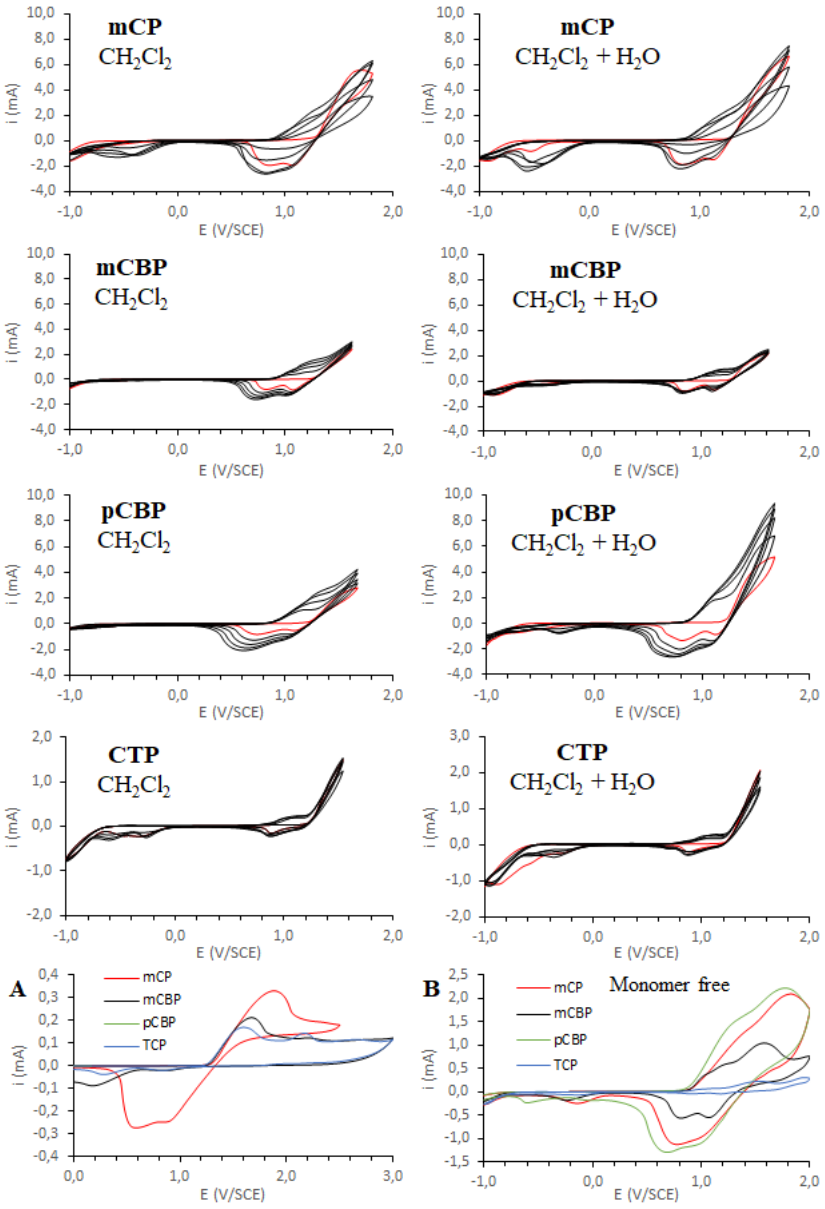

Figure 2. Cyclic voltammograms at scan rate 20mV/s of mCP, mCBP, pCBP and CTP in CH_2Cl_2 and CH_2Cl_2+H_2O, with Bu_4NClO_4 as electrolyte and 5 mM monomer. Red line represents the first cycle and black lines subsequent 4 scans. In particular, A: CV until 3 V/SCE in CH_2Cl_2, B: CV of polymers films on gold slide in monomer-free solution of Bu_4NClO_4 in CH_2Cl_2. (colors refer to the online version)

3.2. Surface morphology

Polymer films were observed by SEM. First, the influence of H_2O content on surface structures is huge. In solvent CH_2Cl_2, the depositions were very smooth especially for mCP and mCBP. (**Figure 3**). This can be explained by the low amount of water traces in dry CH_2Cl_2. The water reduction still take place, as seen on the CV curves (**Figure 2**) but the H_2 bubbles are so rare that the soft template is ineffectual, and the polymer depositions stay smooth. pCBP

exhibited anyway rough cauliflowers structures, but no porous structures which are the sign of water reduction.

In CH_2Cl_2+H_2O, more porous structures are observed. mCP depositions showed extremely ordered vertically aligned nanotubes capped with flower-like structures (**Figure 4**) and pCBP also formed long horizontal fibers but with cauliflower like nanoparticles on them (**Figure 3**). On the contrary, mCBP and CTP structures morphologies were more spherical with nanocups and particles. These results can be related to the fact that mCP and pCBP polymerized better than the two others (as already described by the higher intensities on the CV curves). If the carbazoles radical cations are less stable, the dimerization can occur quicker and lead to a rougher polymer deposition. The polymer structures are thus growing in length toward nanotubes and fibers. The structures morphology of the polymer films are therefore very dependent on the molecular structure of the monomer. Moreover, with mCP, the formation the flower-like structures formed on the top of the nanotubes (**Figure 4**) may be explained by a two-step process: In the first scans, only nanotubes are formed because bubbles of nanometric size are released on the substrate. Then, extremely long vertically aligned nanotubes are formed because the growth is first mono-dimensional (1-D). However, when the numbers of scans increase, a huge number of H_2 bubbles are released not only from H_2O trace but also from H^+ formed from monomer oxidation and polymerization. As a consequence, the 1-D growth is hindered and the growth becomes 2-D and even 3-D with the formation of nanosheets and hollow spheres. Indeed, Margaritondo and co-workers already demonstrated by real-time microradiography during electropolymerization of pyrrole in water that the three-phase boundary can change with the presence of bubbles leading to various surface structures [17].

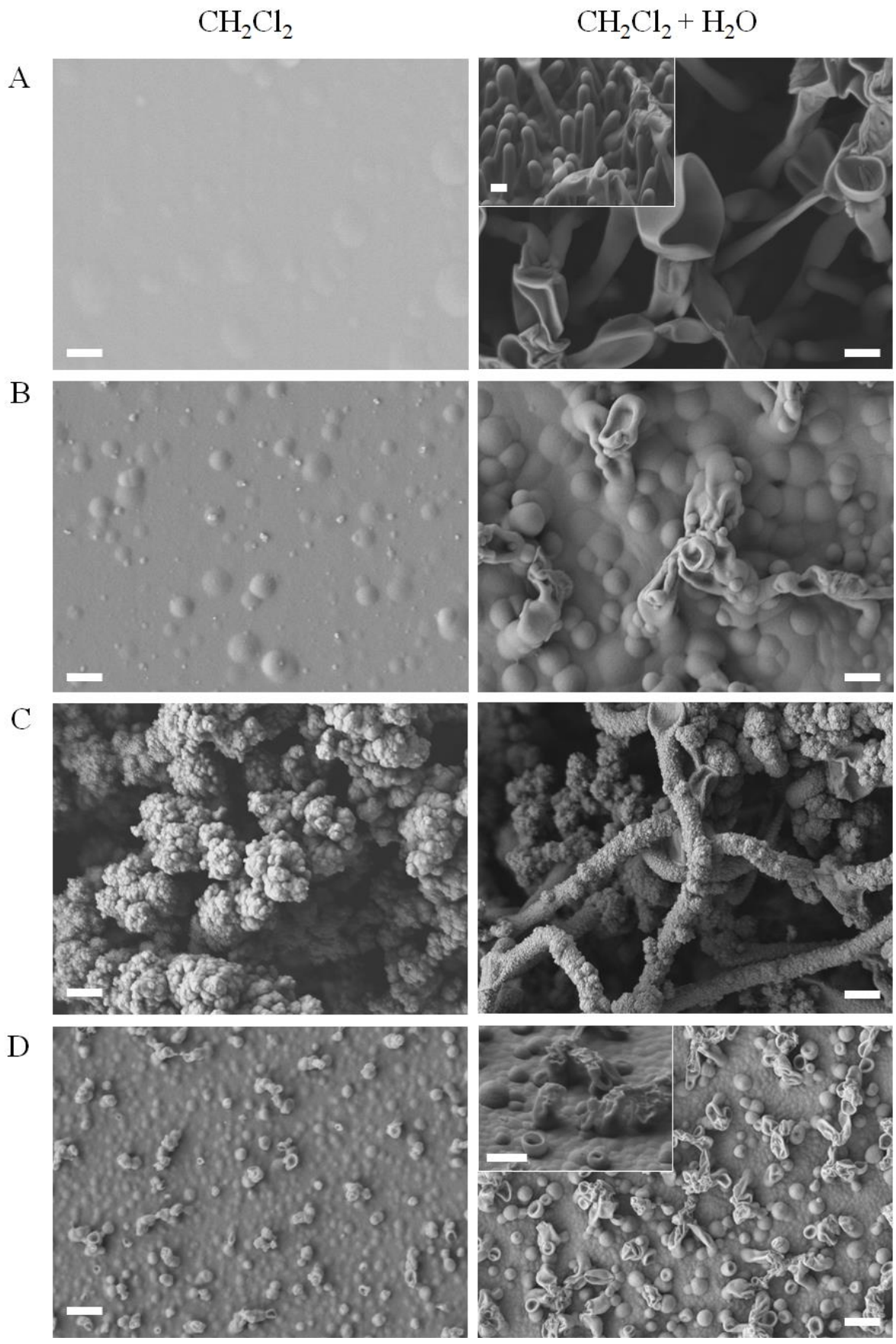
CH_2Cl_2
$CH_2Cl_2 + H_2O$
A
B
C
D

Figure 3. SEM pictures (magnification X10000) of (A) mCP, (B) mCBP, (C) pCBP and (D) CTP, 3 scans depositions in CH_2Cl_2 and CH_2Cl_2+H_2O. Insets show same polymer films with a slope. All scale bars are 1µm long.

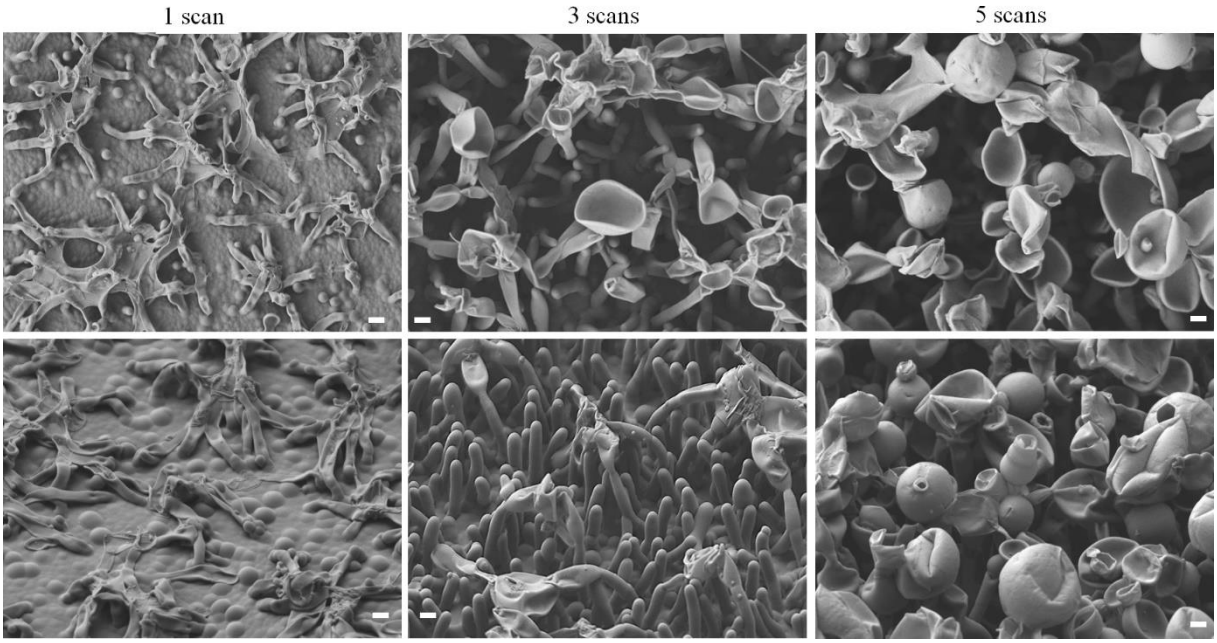

Figure 4. SEM pictures (magnification X5000) of mCP films at different scans depositions in CH_2Cl_2+H_2O, with (down) and without (up) inclination. All scale bars are 1µm long.

Monomers were also electropolymerized at constant potential. As seen on SEM pictures (**Figure 3 and 5**) the structures morphologies can be different depending on the electropolymerization method. This is expected because at constant potential only O_2 bubbles can be released by water while by cyclic voltammetry here H_2 bubbles are released. The surface morphology of mCP is relatively close than that observed by cyclic voltammetry but with mCP the structures change from vertically nanotubes to ribbon-like structures, and for CTP a large deposition charge leads to a porous membrane. Such change in surface morphology was already observed in the literature by changing the monomers but not the deposition method [25].

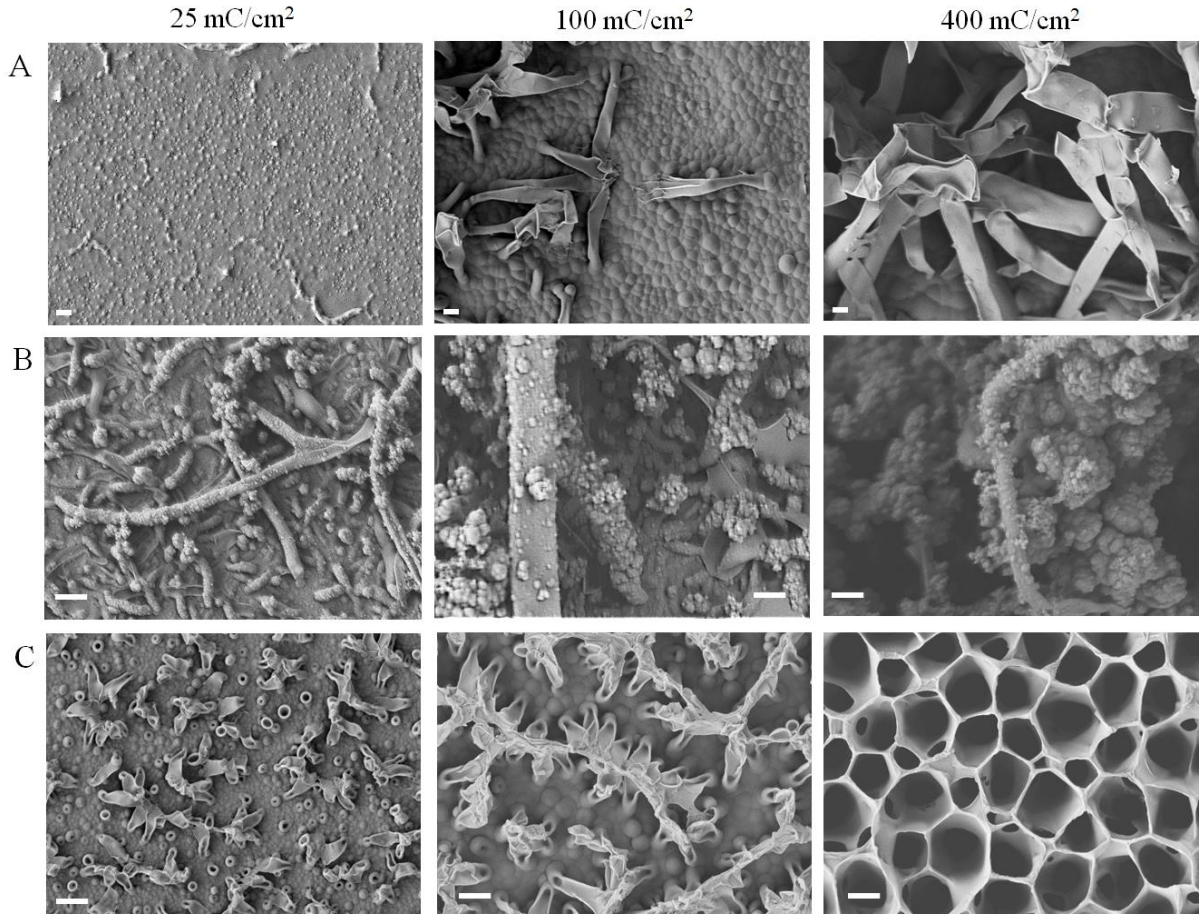

Figure 5. SEM pictures of (A) mCP (magnification X5000), (B) pCBP (X10000), (C) CTP (X10000) depositions at constant potential and different deposition charges in CH_2Cl_2+H_2O. All scale bars are 1µm long.

3.3. Wetting properties

The hydrophobicity of the polymer films was measured through the contact angles of water droplets (**Table 2**). The calculated surface energy γ_S (**Table 1 Supporting Information**) of the films being very similar, the differences in wettability between the films are driven by their roughness and nanostructures shapes.

The surfaces obtained in CH_2Cl_2 were rarely hydrophobic due of their smooth morphology (**Figure 3**) and little roughness (**Table 2 Supporting Informations**), except for pCBP which rough surfaces showed superhydrophobic properties with a static contact angle up to 160 ± 3°. pCBP surfaces were so slippery that for some of them, the droplet couldn't stay on the surface (**Table 2, Figure 6**). The slippery dynamic behavior is associated with a Cassie-

Baxter state [10], confirming that the increasing roughness and amount of air trapped in the nanostructures led to a higher apparent contact angle and low hysteresis.

Surfaces realized in CH_2Cl_2+H_2O are in large majority hydrophobic, highly hydrophobic for mCBP (140 ± 11°) and CTP (136 ± 4°) (**Figure 7**). Since the contact angle of all smooth depositions is less than 90° (**Table 1 Supporting Information**), the fact that the roughness seems to increase with the hydrophobicity is incompatible with a Wenzel state. Dynamic contact angles are nevertheless higher than 90°, exhibiting a parahydrophobic behavior,[11] which seems conflicting with a Cassie-Baxter state. Thus, the high water adhesion properties of the polymer surfaces may be due to a mixed state between Wenzel and Cassie-Baxter.[9,10] Only pCBP needed a larger droplet volume to perform the dynamic angles measurements and seemed to head toward a Cassie-Baxter state.

Polymer	Number of CV scans	Solvent	θ_w [deg]	θ_{adv} [deg]	θ_{rec} [deg]	H [deg]	α [deg]
mCP	1	CH_2Cl_2	80 ± 7	77 ± 4	69 ± 1	8	> 90
	3	CH_2Cl_2	87 ± 7	72 ± 9	73± 4	1	> 90
	5	CH_2Cl_2	**	**	**	**	**
	1	CH_2Cl_2 + H_2O	121 ± 6	127 ± 1	116 ± 1	11	> 90
	3	CH_2Cl_2 + H_2O	78 ± 7	66 ± 4	57 ± 4	9	> 90
	5	CH_2Cl_2 + H_2O	114 ± 9	119 ± 1	109 ± 3	10	> 90
mCBP	1	CH_2Cl_2	96 ±1	92 ± 1	88 ± 1	4	> 90
	3	CH_2Cl_2	101 ± 2	94 ± 2	87 ± 3	7	> 90
	5	CH_2Cl_2	101 ± 1	99 ± 4	89 ± 3	10	> 90
	1	CH_2Cl_2 + H_2O	82 ± 5	99 ± 9	81 ± 13	18	> 90
	3	CH_2Cl_2 + H_2O	127 ± 8	132 ± 7	111 ± 17	21	> 90
	5	CH_2Cl_2 + H_2O	140 ± 11	161 ± 1	113 ± 1	48	> 90
pCBP	1	CH_2Cl_2	125 ± 4	125 ± 3	111 ± 2	14	> 90*
	3	CH_2Cl_2	146 ± 1	158 ± 4	117 ± 4	41	55 ± 3
	5	CH_2Cl_2	160 ± 3	*	*	*	0
	1	CH_2Cl_2 + H_2O	80 ± 9	87 ± 8	56 ± 10	31	> 90
	3	CH_2Cl_2 + H_2O	114 ± 6	122 ± 8	106 ± 3	16	> 90
	5	CH_2Cl_2 + H_2O	99 ± 8	94 ± 1	86 ± 2	8.0	> 90*
CTP	1	CH_2Cl_2	90 ±6	85 ± 6	81 ± 5	4	> 90
	3	CH_2Cl_2	104 ± 3	98 ± 9	92 ± 11	6	> 90
	5	CH_2Cl_2	99 ± 5	98 ± 16	98 ± 5	0	> 90

1	CH_2Cl_2 + H_2O	104 ± 4	98 ± 5	83 ± 14	15	> 90
3	CH_2Cl_2 + H_2O	136 ± 4	125 ± 6	112 ± 2	13	> 90
5	CH_2Cl_2 + H_2O	135 ± 7	148 ± 20	123 ± 12	25	> 90

Table 2. Static and dynamic contact angle measurements. (*: impossible measurement because the drop doesn't stay on the substrate) (**: stripes on the substrate disrupt the measurement) (>90*: the droplet volume needed to be increased to perform the measurement)

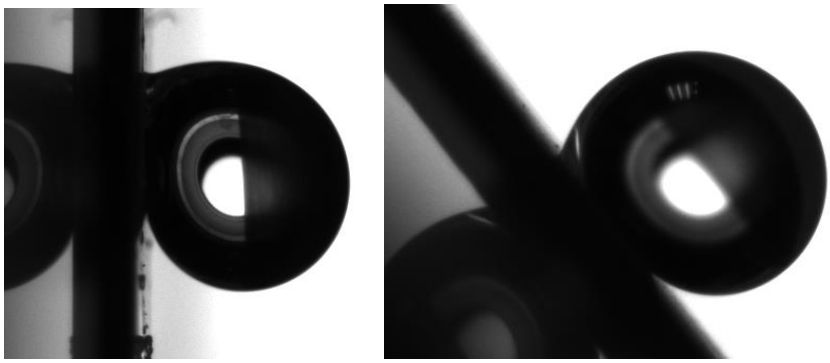

Figure 6. Dynamic contact angles measurements (left mCBP and right pCBP).

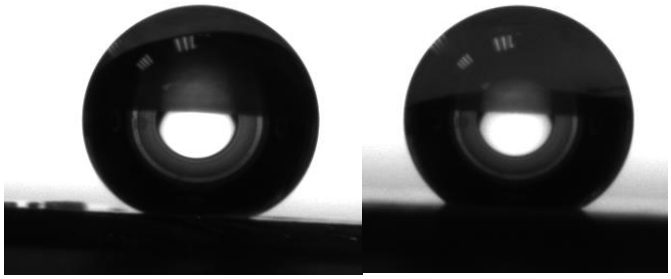

Figure 7. Static contact angles measurements (left mCBP and right CTP, 5 scans CH_2Cl_2 + H_2O).

4. Conclusion

In this article, we demonstrated for the first time that conjugated carbazole monomers are excellent alternatives to thiophene-based molecules that were reported for their high capacity to form nanostructured polymer films using a surfactant-free soft-template electropolymerization in organic solvent [23-29]. We demonstrated that the presence of water in the solvent had a huge impact on the shape of the structures while the molecular nature of the monomer was the main factor determining the morphologies of the nanostructures. Different

morphologies were obtained from fibers to vertically aligned nanotubes but also vertically aligned nanotubes capped with flower-like structures with mCP, which may be due to a two-step process. The rough surfaces were highly parahydrophobic, except for pCBP which exhibit slippery behaviors typical of a Cassie-Baxter state. Many applications could be envisaged for such parahydrophobic surfaces in water harvesting, opto-electronic devices or sensors. Moreover, various substituents could be grafted in the future and especially on nitrogen of carbazole if monomers with NH groups are studied.

5. Acknowledgment

The authors would like to acknowledge *Agence Innovation Défense* for their grant and support. The group thanks Christelle Boscagli from the Centre Commun de Microscopie Appliquée (CCMA, Université Côte d'Azur) for the preparation of the substrates necessary for the SEM analyses. IR analyses were performed at the Smart City Innovation Center (Université Côte d'Azur, IMREDD). The "Smart City Innovation Center" is a project funded by the European union with the European fund for regional development and co-funded by Métropole Nice Côte d'Azur, the département Alpes-maritimes, the région Sud Provence-Alpes-Côte and France for the "initiative d'excellence" (Investissements d'avenir). This work has been supported by CNRS GDR 2088 « BIOMIM ».

6. References

[1] Y. Cheng, H. Yang, Y. Yang, J. Huang, K. Wu, Z. Chen, X. Wang, C. Lin, Y. Lai, Progress in TiO_2 nanotube coatings for biomedical applications: A review, J. Mater. Chem. B 6 (2018) 1862−1886.

[2] V. Chaudhery, S. George, M. Lu, A. Pokhriyal, B.T. Cunningham, Nanostructured surfaces and detection instrumentation for photonic crystal enhanced fluorescence, Sensors 13 (2013) 5561−5584.

[3] S. Tawfick, M. De Volder, D. Copic, S.J. Park, C.R. Oliver, E.S. Polsen, M.J. Roberts, A.J. Hart, Engineering of micro- and nanostructured surfaces with anisotropic geometries and properties, Adv. Mater. 24 (2012) 1628–1674.

[4] Z. Cheng, J. Gao, L. Jiang, Tip geometry controls adhesive states of superhydrophobic surfaces, Langmuir 26 (2010) 8233−8238.

[5] A. Al-Azawi, M. Latikka, V. Jokinen, S. Franssila, R.H.A. Ras, Friction and wetting transitions of magnetic droplets on micro-pillared superhydrophobic surfaces, Small 13 (2017) 1700860.

[6] T. Darmanin, F. Guittard, Superhydrophobic and superoleophobic properties in Nature, Mater. Today 18 (2015) 273−285.

[7] S. Yu, Z. Guo, W. Liu, Biomimetic transparent and superhydrophobic coatings: From nature and beyond nature, Chem. Commun. 51 (2015) 1775−1794.

[8] B. Su, Y. Tian, L. Jiang, Bioinspired interfaces with superwettability: From materials to chemistry, J. Am. Chem. Soc. 138 (2016) 1727–1748.

[9] R.N. Wenzel, Resistance of solid surfaces to wetting by water, Ind. Eng. Chem. 28 (1936) 988–994.

[10] A.B.D. Cassie, S. Baxter, Wettability of porous surfaces, Trans. Faraday Soc. 40 (1944) 546–551.

[11] A. Marmur, Hydro- hygro- oleo- omni-phobic? Terminology of wettability classification, Soft Matter 8 (2012) 6867−6870.

[12] C.W. Extrand, Origins of wetting, Langmuir 32 (2016) 7697–7706.

[13] W. Barthlott, C. Neinhuis, Purity of the sacred lotus, or escape from contamination in biological surfaces, Planta 202 (1997) 1.

[14] Non wettable surfaces: Theory, preparation, and applications, Chapter 3, RSC Soft Matter No.5, Edited by A. Marmur and R.H.A. Ras, The Royal Society of Chemistry 2017.

[15] L. Lee, S.J. Park, Porous anodic aluminum oxide: Anodization and templated synthesis of functional nanostructures, Chem. Rev. 114 (2014) 7487–7556.

[16] H.-A. Lin, S.-C. Luo, B. Zhu, C. Chen, Y. Yamashita, H.-h. Yu, Molecular or nanoscale structures? The deciding factor of surface properties on functionalized poly(3,4ethylenedioxythiophene) nanorod arrays, Adv. Funct. Mater. 23 (2013) 3212–3219.

[17] S. Gupta, Hydrogen bubble assisted syntheses of polypyrrole micro/nanostructures using electrochemistry: Structural and physical property characterization, J. Raman Spectrosc. 39 (2008) 1343–1355.

[18] J.T. Kim, S.K. Seol, J.H. Je, Y. Hwu, G. Margaritondo, The microcontainer shape on electropolymerization bubbles, Appl. Phys. Lett. 94 (2009) 034103.

[19] C. Debiemme-Chouvy, Template-free one-step electrochemical formation of polypyrrole nanowire array, Electrochem. Commun. 11 (2009) 998–301.

[20] A. Fakhry, H. Cachet, C. Debiemme-Chouvy, Mechanism of formation of templateless electrogenerated polypyrrole nanostructures, Electrochim. Acta 179 (2015) 297–303.

[21] B. Parakhonskiy, D. Shchukin, Polypyrrole microcontainers: Electrochemical synthesis and characterization, Langmuir 31 (2015) 9214−9218.

[22] L. Qu, G. Shi, F. Chen, J. Zhang, Electrochemical growth of polypyrrole microcontainers, Macromolecules 36 (2003) 1063−1067.

[23] C.R. Szczepanski, I. M'Jid, T. Darmanin, G. Godeau, F. Guittard, Template-free approach to nanotube-decorated polymer surfaces using 3,4-phenylenedioxythiophene (PhEDOT) monomers, J. Mater. Chem. A 4 (2016) 17308–17323.

[24] G. Ramos Chagas, F. Guittard, T. Darmanin, One-step and templateless electropolymerization process using thienothiophene derivatives to develop arrays of nanotubes and tree-like structures with high water adhesion, ACS Appl. Mater. Interfaces 8 (2016) 22732–22743.

[25] T. Darmanin, E.L. Klimareva, I. Schewtschenko, F. Guittard, I.F. Perepichka, Exceptionally strong effect of small structural variations in functionalized 3,4-phenylenedioxythiophenes on the surface nanostructure and parahydrophobic properties of their electropolymerized films, Macromolecules 52 (2019) 8088–8102.

[26] E.h.Y. Thiam, A. Dramé, S. Sow, A. Sene, C.R. Szczepanski, S.Y. Dieng, F. Guittard, T. Darmanin, Designing nanoporous membranes through templateless electropolymerization of thieno[3,4-b]thiophene derivatives with high water content, ACS Omega 4 (2019) 13080−13085.

[27] O. Sane, A. Diouf, G. Morán Cruz, F. Savina, R. Méallet-Renault, S. Amigoni, S.Y. Dieng, F. Guittard, T. Darmanin, Coral-like nanostructures, Mater. Today 31 (2019) 119–120.

[28] M. Khodja, M. El Kateb, M. Beji, F. Guittard, T. Darmanin, Tuning nanotubular structures by templateless electropolymerization with thieno[3,4-b]thiophene-based monomers with different substituents and water content, J. Colloid Interface Sci. 564 (2020) 19–27.

[29] F. Sow, A. Dramé, S. Sow, A. Sene, F. Orange, S.Y. Dieng, F. Guittard, T. Darmanin, Influence of spacer in the formation of nanorings by templateless electropolymerization. Mater. Today Chem. 17 (2020) 100278.

[30] T. Darmanin, F. Guittard, Molecular design of conductive polymers to modulate superoleophobic properties, J. Am. Chem. Soc. 131 (2009) 7928–7933.

[31] I. Bousrih, M. El Kateb, C.R. Szczepanski, M. Beji, F. Guittard, T. Darmanin, A bioinspired strategy for designing well-ordered nanotubular structures by templateless electropolymerization of thieno[3,4-b]thiophene-based monomers, Phil. Trans. R. Soc. A 378 (2020) 20190450.

[32] K. Karon, M. Lapkowski, Carbazole electrochemistry: A short review, J. Solid State Electrochem. 19 (2015) 2601–2610.

[33] D. Kolosov, V. Adamovich, P. Djurovich, M.E. Thompson, C. Adachi, 1,8-Naphthalimides in phosphorescent organic LEDs: The interplay between dopant, exciplex, and host emission, J. Am. Chem. Soc. 124 (2002) 9945–9954.

[34] T. Thoms, S. Okada, J.-P. Chen, M. Furugori, Improved host material design for phosphorescent guest–host systems, Thin Solid Films 436 (2003) 264–268.

[35] S. Gong, X. He, Y. Chen, Z. Jiang, C. Zhong, D. Ma, J. Qin, C. Yang, Simple CBP isomers with high triplet energies for highly efficient blue electrophosphorescence, J. Mater. Chem. 22 (2012) 2894–2899.

[36] J. Lee, J.-I. Lee, J.Y. Lee, H.Y. Chu, Enhanced efficiency and reduced Roll-off in blue and white phosphorescent organic light-emitting diodes with a mixed host structure, Appl. Phys. Lett. 94 (2009) 193305.

[37] Q. Chen, D.P. Liu, M. Luo, L.J. Feng, Y.C. Zhao, B.H. Han, Nitrogen-containing microporous conjugated polymers via carbazole-based oxidative coupling polymerization: Preparation, porosity, and gas uptake, Small 10 (2014) 308–315.

[38] Y. Zhi, S. Ma. H. Xia, Y. Zhang, Z. Shi, Y. Mu, X. Liu, Construction of donor-acceptor type conjugated microporous polymers: A fascinating strategy for the development of efficient heterogeneous photocatalysts in organic synthesis. Appl. Catal. B-Environ. 244 (2019) 36–44.

[39] D. Taylor, S.J. Dalgarno, Z. Xu, F. Vilela, Conjugated porous polymers: incredibly versatile materials with far-reaching applications. Chem. Soc. Rev. 49 (2020) 3981-4042.

[40] S. Sow, F. Sow, A. Dramé, F. Orange, A. Sene, S.Y. Dieng, F. Guittard, T. Darmanin, Influence of alkyl spacer in nanostructure shape control by templateless electropolymerization. Prog. Org. Coat. 146 (2020) 105698.

[41 S. Wu « Calculation of Interfacial Tension in Polymer Systems », J. Polymer Science, 34, 1971, pp19-30.

[42] M.I. Mangione, R.A. Spanevello, D. Minudri, P. Cavallo, L. Otero, F. Fungo, Electrochemical films deposition and electro-optical properties of bis-carbazol-triphenylamine end-capped dendrimeric polymers, Electrochim. Acta 263 (2018) 585–595.

[43] M.I. Mangione, R.A. Spanevello, D. Minudri, D. Heredia, L. Fernandez, L. Otero, F. Fungo, Electropolymerization of functionalized carbazole end-capped dendrimers. Formation of conductive films, Electrochim. Acta 207 (2016) 143–151.

[44] K. Karon M. Lapkowski, G. Juozas, Electrochemical and UV-Vis/ESR spectroelectrochemical properties of polymers obtained from isomeric 2,7- and 3,6- linked carbazole trimers; influence of the linking topology on polymers properties, Electrochim. Acta 123 (2014) 176–182.

Figures captions:

Figure 1. Monomers studied in this manuscript.

Figure 2. Cyclic voltammograms at scan rate 20mV/s of mCP, mCBP, pCBP and CTP in CH_2Cl_2 and CH_2Cl_2+H_2O, with Bu_4NClO_4 as electrolyte and 5 mM monomer. Red line represents the first cycle and black lines subsequent scans. In particular, A: CV until 3 V/SCE in CH_2Cl_2, B: CV of polymers films on gold slide in monomer-free solution of Bu_4NClO_4 in CH_2Cl_2. (colors refer to the online version)

Figure 3. SEM pictures (magnification X10000) of (A) mCP, (B) mCBP, (C) pCBP and (D) CTP, 3 scans depositions in CH_2Cl_2 and CH_2Cl_2+H_2O. Insets show same polymer films with a slope. All scale bars are 1µm long.

Figure 4. SEM pictures (magnification X5000) of mCP films at different scans depositions in CH_2Cl_2+H_2O, with (down) and without (up) inclination. All scale bars are 1µm long.

Figure 5. SEM pictures of (A) mCP (magnification X5000), (B) pCBP (X10000), (C) CTP (X10000) depositions at constant potential and different deposition charges in CH_2Cl_2+H_2O. All scale bars are 1µm long.

Figure 6. Dynamic contact angles measurements (left mCBP and right pCBP).

Figure 7. Static contact angles measurements (left mCBP and right CTP, 5 scans CH_2Cl_2 + H_2O).

Tables captions:

Table 1: Electrochemical properties of the monomers and the polymers films.

Table 2. Static and dynamic contact angle measurements. (*: impossible measurement because the drop doesn't stay on the substrate) (**: stripes on the substrate disrupt the measurement) (>90*: the droplet volume needed to be increased to perform the measurement)